buildings

MDPI

Article

Rethinking Climatic Adaptation for Residential Building Energy Efficiency: Cross-Regional Comparative Analysis for Envelope Insulation in China

Yang Yang [1], Junhui Zou [1], Zhineng Jin [2], Yiheng Liu [1,*] and Qianru Yang [3,*]

[1] School of Architecture and Design, Southwest Minzu University, Chengdu 610225, China; 13398432841@163.com (Y.Y.); 18161287967@163.com (J.Z.)
[2] State Key Laboratory of Climate Resilience for Coastal Cities, Department of Civil and Environmental Engineering, The Hong Kong University of Science and Technology, Hong Kong, China; zjinbe@connect.ust.hk
[3] AI+Arch Lab, Southwest Minzu University, Chengdu 610225, China
* Correspondence: ianno_0201@163.com (Y.L.); yangqianru@swun.edu.cn (Q.Y.); Tel.: +86-156-8001-6301 (Q.Y.)

Abstract

Envelope-parameter optimization for residential buildings is strongly climate-dependent, yet previous studies have mainly focused on single parameters or specific regions, limiting cross-climate comparison of parameter priorities. This study establishes a unified DeST-based residential building model to compare the effects of external wall insulation thickness and external surface solar absorptivity on heating load, cooling load, annual total load, and operational carbon emissions across five representative climate zones in China. Yinchuan, Beijing, Chengdu, Guangzhou, and Kunming were selected as case cities. Single-factor analysis, two-parameter coupling analysis, supplementary sensitivity analysis, and load-to-carbon translation were conducted under consistent building prototypes, operating boundaries, and evaluation indices. The results show that the effects of the two parameters differ markedly across climate zones, reflecting a transition in parameter dominance under different heating–cooling load structures. Over the tested ranges, insulation thickness changes annual total load by up to approximately 10%, whereas solar absorptivity changes it by only 0.17–1.91%. Mechanistically, insulation reduces winter heat loss but may suppress summer heat dissipation, while solar absorptivity directly affects exterior-surface solar heat gains. Further carbon analysis shows that load-optimal configurations do not necessarily correspond to carbon-optimal configurations. These findings provide quantitative support for climate-adaptive and low-carbon envelope design.

Keywords: residential building envelope; insulation; solar absorption; thermal load; climate adaptability; multi-climate-zone

Check for updates

Academic Editor: Chi Yan Tso

Received: 7 June 2026
Revised: 3 July 2026
Accepted: 8 July 2026
Published: 10 July 2026

1. Introduction

1.1. Background

Against the backdrop of continuously growing global energy consumption and the accelerating transition toward a low-carbon economy, energy conservation and emission reduction in the building sector have become an essential component of sustainable development [1]. As of 2021, the building sector accounted for 37% of global carbon dioxide emissions and 36% of global energy consumption, and this share is projected to exceed 50% by 2050 [2]. Moreover, the building operation stage requires substantial long-term energy consumption to maintain the indoor thermal environment, among which air-conditioning-related loads, such as heating and cooling, constitute a major share of operational energy use in buildings [3]. According to statistics, HVAC systems account for 40–50% of total building energy consumption [4,5]. Therefore, reducing heating and cooling loads during the operational stage is one of the key approaches to achieving energy conservation and carbon reduction in buildings.

Among various building types, residential buildings are large in number, widely distributed, and closely connected to daily life, making their operational energy consumption highly prevalent and persistent [6]. According to relevant data, residential buildings account for approximately 10% of the global energy supply, with an annual growth rate of about 1.5% [7]. Building envelope is the primary interface for heat exchange between a building and the outdoor environment. Its thermal performance directly affects the control of heat loss in winter and the mitigation of solar heat gains in summer, thereby exerting a significant influence on annual energy loads [8,9]. Among envelope parameters, external wall insulation performance and external surface solar-radiation characteristics have particularly direct effects on building thermal loads. Increasing the insulation thickness of external walls can improve the thermal resistance of the envelope and reduce heat loss in winter, but it may also alter cooling loads in summer [10]. External surface solar absorptivity determines the extent to which the building envelope absorbs solar radiation, and a higher absorptivity generally increases solar heat gains and cooling demand in summer [11]. These two parameters represent the envelope's capacity for heat-transfer resistance and solar-radiation response, respectively, and play important roles in the annual energy performance of buildings.

However, the effects of envelope parameters on building thermal loads are not consistent across all regions. Significant differences exist among China's climate zones in terms of outdoor temperature, solar radiation, and the composition of heating and cooling demands, which means that the same envelope parameter may exhibit different energy-saving effects in different regions [12,13]. Therefore, the optimization of envelope parameters should not follow a uniform strategy; instead, it should be analyzed in light of specific climatic conditions to reveal the influence patterns of typical envelope parameters on residential building thermal loads and to provide a basis for optimized design.

1.2. Literature Review

External wall insulation thickness. A first body of work establishes that insulation thickness reshapes both heating and cooling energy use, with effects that are strongly climate-conditioned. Pan et al. showed that varying insulation thickness affects annual heating and cooling consumption differently across climates [10], and Zhang et al. found that increasing thickness reduces heating loads more markedly while the optimal wall configuration shifts by region [14]. Across 32 Chinese regions, Yuan et al. demonstrated pronounced spatial variation in optimum thickness, closely tied to energy-saving and carbon-reduction benefits [15], and Kaynakli's review confirmed that climatic conditions have consistently governed thickness selection alongside economic performance [16].

External surface solar absorptivity. A second body of work addresses the radiative response of the envelope surface. Ozel reported that higher solar absorptivity raises cooling loads, lowers heating loads, and shifts the optimum insulation thickness [11]. Kontoleon and Eumorfopoulou showed that absorptivity, coupled with orientation, alters wall time lag and decrement factor and hence the dynamic thermal response [17], while Košir et al. found that its effect on total energy use intensifies when envelope thermal performance is weak [18]. Rosado and Levinson confirmed for cool walls that raising exterior reflectance lowers warm-season cooling demand but can incur a heating penalty in colder climates [19].

Simulation-based and climate-adaptive envelope studies. A third strand couples building-performance simulation with cross-regional analysis. The integrated DeST platform simulates building and HVAC behavior jointly [20], and DeST 3.0 adds advanced envelope, occupant, and energy-system modules verified through code checking, program comparison, and case calibration [21]. On this basis, Pan et al. argued that envelope strategies should follow local load characteristics [22]; Zhang et al. modeling 1677 Chinese cities, revealed clear spatial heterogeneity in how envelope upgrades affect demand [23]; and Duan et al. showed that passive-house envelope performance and optimum insulation vary by zone and internal-gain intensity [24]. Importantly, Meng et al. noted that existing work over-emphasizes insulation level while under-comparing the relative effects of different envelope parameters, indicating that dominant-parameter identification within a unified framework remains underdeveloped [25].

Collectively, these studies establish the directional effects of each parameter but rarely place insulation thickness and solar absorptivity on a common, quantitatively comparable footing across China's full set of climate zones—the gap this study addresses.

1.3. Research Focus

As discussed above, previous studies have revealed the effects of external wall insulation thickness, external surface solar absorptivity, and climatic conditions on building heating and cooling loads from different perspectives, thereby providing an important basis for climate-adaptive envelope design. However, existing research has mostly focused on the energy-saving effects of single parameters, specific regions or boundary conditions. Further investigation is still needed to compare the direction, magnitude, and relative dominance of different envelope parameters across multiple climate zones under a unified building prototype, consistent operating boundaries, and common evaluation indices.

Therefore, this study does not seek a universal envelope configuration for all climate zones. Instead, it uses a unified DeST reference model to compare the load responses of external wall insulation thickness and external surface solar absorptivity across China's five major climate zones. It further examines parameter dominance transitions and the relationship between load-optimal and operational carbon-optimal configurations. The main contributions are as follows:

1. A unified cross-climate-zone comparative framework is established: Under consistent modelling boundaries, building prototype, operating conditions, and evaluation indices, the effects of external wall insulation thickness and external surface solar absorptivity are compared on the same scale, improving the horizontal comparability of results across climate zones.
2. The relative effect magnitude and dominance transition of the two envelope parameters are quantitatively identified: Rather than only determining whether each parameter affects building loads, this study further clarifies how strongly the two parameters affect annual total load and how their dominance changes with different heating–cooling load structures.
3. The relationship between load-optimal and operational carbon-optimal configurations is further examined: Thermal-load optimization results are further translated into operational carbon emissions and compared with engineering standards. The consistency and divergence between load-optimal and carbon-optimal configurations are examined, thereby providing more practice-oriented guidance for residential envelope design and energy-efficiency retrofits in different climate zones.

Figure 1 presents the overall research framework of this study. The workflow includes representative city selection, unified reference-model construction, envelope-parameter simulation, supplementary sensitivity analysis, and operational carbon estimation.

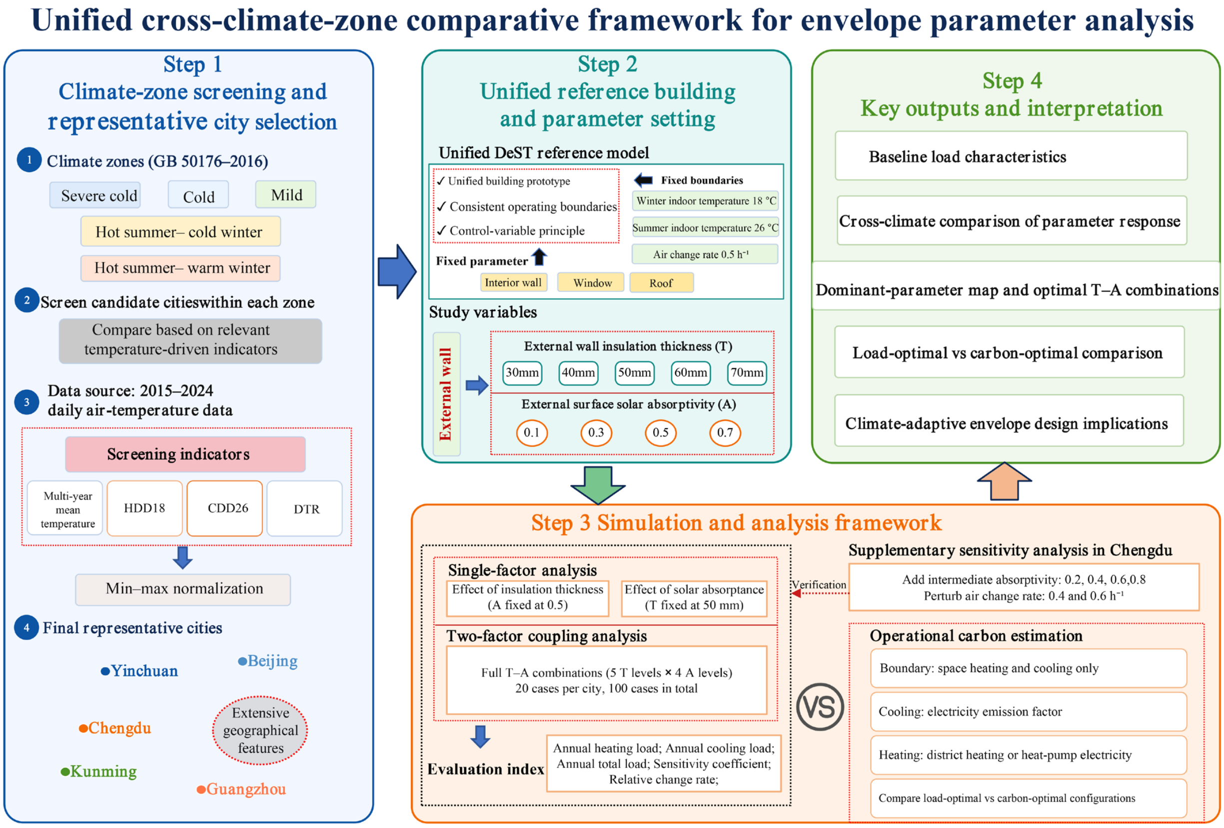

Figure 1. Research framework of the study.

2. Methodology

2.1. Model Construction and Parameter Setting

In this study, an existing multi-story residential building project was selected as the prototype, and a unified reference model was established using DeST software (Version 20230713, Tsinghua University, Beijing, China). Based on this model, simulation analyses were conducted to investigate the effects of envelope parameters on building thermal loads across different climate zones. DeST performs dynamic thermal calculations based on building heat balance and hourly meteorological data, enabling the simulation of heating and cooling loads under specified envelope and operating conditions [26]. The reference building consists of six stories, with a floor height of 3.6 m, a total floor area of 2025.84 m^2, a rectangular plan layout, and a due-south orientation. The model is illustrated in Figure 2.

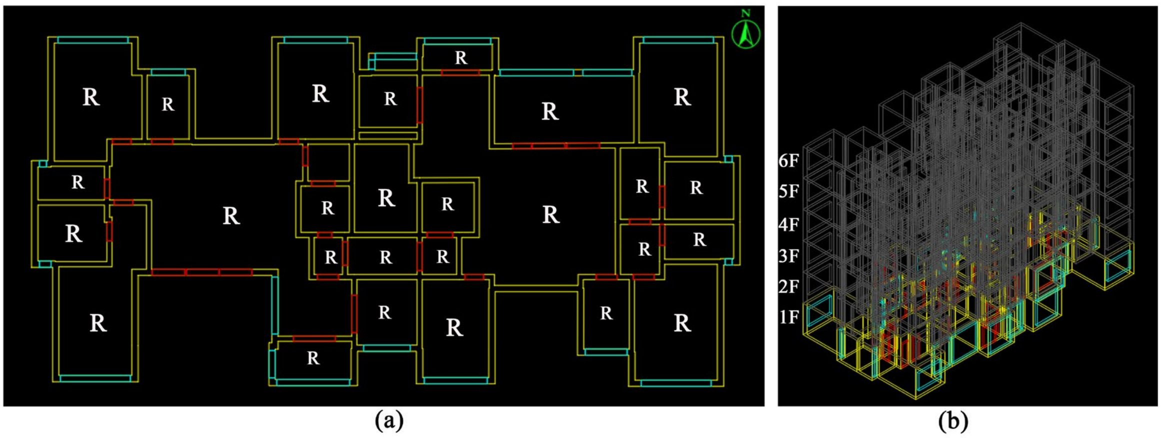

Figure 2. Reference residential building model: (**a**) standard floor plan; (**b**) three-dimensional view.

Building envelope was modeled based on the original project specifications. The basic exterior wall assembly consisted of 20 mm cement mortar + 200 mm red clay brick + polystyrene foam insulation + 20 mm cement mortar, in which the insulation thickness was taken as a study variable and varied from 30 to 70 mm, with the corresponding thermal transmittance of the exterior wall adjusted accordingly. The interior wall assembly consisted of 20 mm cement mortar + 180 mm expanded clay aggregate concrete + 20 mm cement mortar, with a thermal transmittance of 1.515. The roof assembly consisted of 80 mm slag concrete + 40 mm expanded polystyrene board + 100 mm reinforced concrete, with a thermal transmittance of 0.814. The external windows were modeled as insulated glass PVC windows and conventional single-pane windows, with thermal transmittance values of 1.8 and 5.7, respectively. It should be noted that although the thermal performance of the external windows may affect the absolute level of thermal loads, it was kept constant across all cities and simulation cases and was therefore not treated as a study variable in this work. Indoor operating boundary conditions were uniformly specified. The indoor design temperature was set at 18 °C in winter and 26 °C in summer, while the air change rate under natural ventilation was set at 0.5 h^{-1}. The detailed parameter settings are presented in Table 1.

Table 1. Model boundary condition setting.

Boundary Conditions		**Setting**	**Heat Transfer Coefficient**
Indoor Conditions	Temperature	Winter: 18 °C	/
		Summer: 26 °C	/
	Air change rate	0.5 h^{-1}	/
Envelope	Exterior wall	20 mm cement mortar + 200 mm red clay brick + polystyrene foam insulation (30–70 mm) + 20 mm cement mortar	30–70 mm: 0.767, 0.659, 0.578, 0.515, 0.409
	Interior wall	20 mm cement mortar + 180 mm expanded clay aggregate concrete + 20 mm cement mortar	1.515
	Roof	80 mm slag concrete + 40 mm expanded polystyrene board + 100 mm reinforced concrete	0.814
Window		Ordinary 6 mm single glass and Insulated glass + PVC windows	5.7 and 1.8

2.2. Climate Zones and Representative Cities

According to the Technical Standard for Thermal Design of Civil Buildings (GB 50176-2016), China is divided into five climate zones: severe cold, cold, hot summer–cold winter, hot summer–warm winter, and mild [27]. Considering China's vast geographical extent, cities within the same climate zone may differ in latitude, topography, land–sea position, and other geographical factors, which may further lead to differences in outdoor temperature, solar radiation, humidity, wind conditions, and diurnal temperature range. Therefore, before determining the final simulation cities, several candidate cities were selected within each climate zone for comparative analysis, so as to improve the rationality of representative city selection.

Since this study focuses on the heating and cooling loads of residential buildings, the selection of case cities was mainly based on temperature-driven indicators that are directly related to building heating and cooling demands. Previous studies have shown that variations in building heating load are largely governed by mean air temperature, which can explain a substantial proportion of heating-load variation [28]. Meanwhile, degree-days are commonly used climatic indicators in building energy design and operation analysis and can characterize the influence of climatic conditions on building heating and cooling demands [29,30]. Therefore, this study used the multi-year mean temperature to represent the overall thermal background of each city, HDD18 to characterize heating-demand intensity, CDD26 to characterize cooling-demand intensity, and DTR to characterize intra-day temperature fluctuation.

Daily near-surface air-temperature data from 2015 to 2024 were obtained from the China Meteorological Data Service Center and used to calculate temperature-related indicators for the candidate cities [31]. The multi-year mean temperature, HDD18, and CDD26 were calculated based on daily mean temperature, while DTR was calculated based on daily maximum and minimum temperatures. HDD18 and CDD26 were first accumulated on a daily basis for each year and then averaged over the 2015–2024 period. The main calculation formulas are as follows:

- Heating and Cooling degree-day:

$$HDD18 = \sum_{d=1}^{n} \max(18 - T_{mean,d},\ 0) \tag{1}$$

$$CDD26 = \sum_{d=1}^{n} \max(T_{mean,d} - 26,\ 0) \tag{2}$$

where $T_{mean,d}$ is the daily mean air temperature on day d, and n is the number of days during the study period. $HDD18$ denotes the heating degree days with a base temperature of 18 °C. $CDD26$ denotes the cooling degree days with a base temperature of 26 °C.

- Diurnal temperature range:

$$DTR = \frac{1}{n}\sum_{d=1}^{n} (T_{max,d} - T_{min,d}) \tag{3}$$

where $T_{max,d}$ and $T_{min,d}$ are the daily maximum and minimum air temperatures on day d, respectively. DTR denotes the average diurnal temperature range during the study period.

Several representative candidate cities were selected within each of the five climate zones for comparative analysis. These cities differ to some extent in geographical location, heating and cooling demand intensity, and diurnal temperature range, making them suitable for comparing the dispersion of temperature-driven heating and cooling demand characteristics within the same climate zone. Table 2 presents the calculated temperature-related indicators of the candidate cities from 2015 to 2024.

To compare indicators with different units and magnitudes, the four indicators were normalized using the min–max method:

- Min–max normalization:

$$X'_{ij} = \frac{X_{ij} - X_{j,min}}{X_{j,max} - X_{j,min}} \tag{4}$$

where X_{ij} is the original value of city i for temperature-related indicator j; $X_{j,min}$ and $X_{j,max}$ are the minimum and maximum values of indicator j among all candidate cities, respectively; and X'_{ij} is the normalized value.

Table 2. Temperature-related indicators of candidate cities in different climate zones of China.

Climatic Zone	City	Annual Mean Temperature (°C)	HDD18 (°C·d)	CDD26 (°C·d)	DTR (°C)
Severe cold	Yinchuan	11.00	3203.2	35.4	15.66
	Hohhot	7.87	4099.9	5.6	18.20
	Shenyang	9.31	3809.3	30.3	15.10
Cold	Xi'an	14.60	2185.2	120.8	14.87
	Beijing	11.99	3032.1	69.6	19.87
	Jinan	13.31	2549.8	58.7	16.78
Hot summer and cold winter	Chengdu	17.13	1327.6	84.3	12.33
	Wuhan	17.97	1449.2	300.8	11.29
	Shanghai	17.97	1355.5	257.7	9.57
Hot summer and warm winter	Guangzhou	23.41	282.2	446.2	11.02
	Xiamen	22.11	379.9	326.6	10.14
	Haikou	24.98	72.3	443.2	8.14
Mild	Kunming	16.49	1050.2	0.1	17.83
	Guiyang	16.14	1509.8	19.7	10.78

Note: The indicators were calculated from daily near-surface air-temperature data from 2015 to 2024. HDD18 and CDD26 denote heating degree days at 18 °C and cooling degree days at 26 °C, respectively. DTR denotes diurnal temperature range.

As shown in Table 3, the mean standard deviation of the normalized indicators in each climate zone ranges from 0.095 to 0.138, with an overall value close to 0.10. This indicates that the candidate cities within the same climate zone show relatively low overall dispersion in temperature-driven heating and cooling demand characteristics. Accordingly, Yinchuan, Beijing, Chengdu, Guangzhou, and Kunming were finally selected as representative case cities for the five climate zones. Spatially, these five cities cover the geographical distribution characteristics of Northwest China, North China, Southwest China, East China, and South China (Figure 3). They can therefore be used to construct typical simulation scenarios under different heating and cooling demand conditions, thereby supporting the subsequent comparison of envelope-parameter responses under a unified building model and consistent boundary conditions.

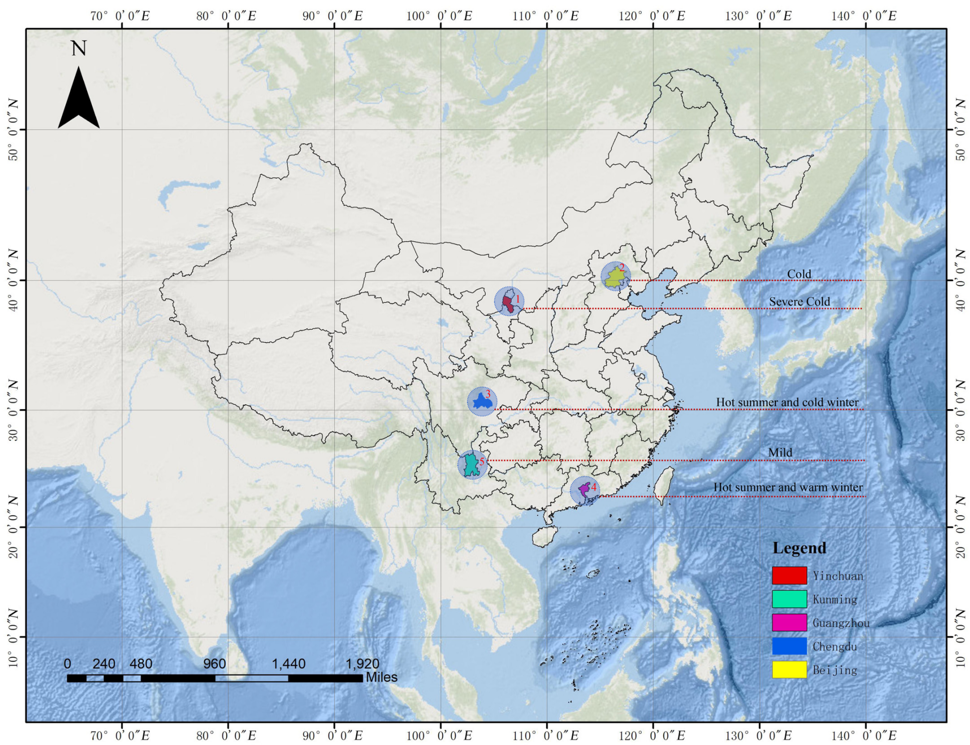

Figure 3. Locations of the selected representative case cities in China.

Table 3. Within-zone dispersion of normalized temperature-related indicators.

Climate	SD of Temperature′	SD of HDD18′	SD of CDD26′	SD of DTR′	Mean SD
Severe cold	0.092	0.114	0.036	0.141	0.095
Cold	0.076	0.105	0.074	0.215	0.118
Hot summer and cold winter	0.028	0.016	0.257	0.119	0.105
Hot summer and warm winter	0.084	0.039	0.153	0.126	0.100
Mild	0.015	0.081	0.031	0.424	0.138

Note: SD denotes standard deviation. The four indicators were first normalized using the min–max method. For each climate zone, the SD of each normalized indicator was calculated among candidate cities, and Mean SD represents the average of the four SD values.

2.3. Simulation Settings and Evaluation Index

2.3.1. Simulation Settings

In this study, the control variable method was adopted to conduct single-factor analysis and two-factor coupling analysis in sequence, with the thickness of the external wall insulation layer and the external surface solar absorptivity taken as the study variables. During the simulations, only these two variables were varied, while all other building configurations, indoor parameters, and operating conditions were kept unchanged.

Building energy-efficiency design standards generally regulate envelope performance through thermal transmittance limits or overall thermal-performance requirements, rather than prescribing a uniform insulation thickness for all climate zones and insulation materials [27]. Following the control-variable principle, this study set the external wall insulation thickness at five levels—30, 40, 50, 60, and 70 mm—as a unified parametric range for comparing load responses across climate zones under the same model and operating conditions. This range is also consistent with the thickness intervals commonly used in previous parametric studies on optimum wall insulation [32]. It should be noted that the purpose of this setting is not to determine code-recommended or cost-optimal thicknesses for each climate zone, but to reveal the load-response mechanism of insulation thickness within a defined parameter space. In particular, for severe cold regions, this range should be interpreted as a controlled comparative setting rather than the complete practical design range.

The external surface solar absorptivity was set at four typical levels: 0.1, 0.3, 0.5, and 0.7. These values were used to represent the variation in solar-radiation absorption of exterior wall finishes from highly reflective to highly absorptive surfaces. Previous studies have also analyzed solar absorptivity within the range of 0–1 at intervals of 0.2, confirming its influence on building thermal performance and load variation [11].

In the single-factor analysis, the external surface solar absorptivity was fixed at 0.5 when investigating the effect of insulation thickness, while the insulation thickness was fixed at 50 mm when examining the effect of solar absorptivity. These fixed values were selected from the intermediate levels of the respective parameter ranges in order to reduce the interference of boundary conditions on the single-factor results and to enhance the comparability of the results obtained for different parameters. In the two-factor coupling analysis, full combinations of insulation thickness and solar absorptivity were considered to examine the total-load response characteristics of different parameter combinations under different climate zones. The detailed simulation scheme is presented in Table 4.

Table 4. Parameter settings for single-factor and dual-factor simulations.

Analysis Level	Content	Setting
Research variable	T	30, 40, 50, 60, 70 mm
	A	0.1, 0.3, 0.5, 0.7
Single-factor	Effect of T	A fixed at 0.5; T varied
	Effect of A	T fixed at 50; A varied
Dual-factor coupling	T–A combination analysis	Full combinations of T and A, with 20 cases per city
Simulation scale	Total number of cases	5 cities, 100 cases in total

Note: T denotes external wall insulation thickness, and A denotes external surface solar absorptivity.

2.3.2. Evaluation Index

To quantitatively evaluate the effects of variations in envelope parameters on building thermal loads, this study introduced two evaluation indices—normalized sensitivity coefficient and relative change rate—based on annual heating load, annual cooling load, and annual total load. The normalized sensitivity coefficient was used to measure the relative response of thermal loads to a unit relative change in a parameter, while the relative change rate was employed to characterize the magnitude of thermal-load variation between different cases. The specific definitions are as follows:

- Normalized sensitivity coefficient

$$S = \frac{\Delta Q / Q_0}{\Delta P / P_0} \tag{5}$$

where S is normalized sensitivity coefficient, and Q_0 is building thermal load under the initial parameter condition, ΔQ is the difference in thermal load between the target and initial condition, P_0 is the initial value of parameter, and ΔP is the change in parameter value. When $S > 0$ indicates that increasing the parameter increases the building thermal load, whereas $S < 0$ indicates the opposite. A larger $|S|$ indicates that is more sensitive to changes in that parameter.

- Relative change rate

$$R = \frac{Q_2 - Q_1}{Q_1} \times 100\backslash\% \tag{6}$$

where R is relative change rate, Q_1 and Q_2 are the building thermal loads under the two compared cases, respectively. When $R > 0$, the thermal load increases; $R < 0$, the thermal load decreases. $|R|$ indicates the magnitude of the change.

In single-factor analysis, Q_1 and Q_2 correspond to the thermal loads at the minimum and maximum parameter levels, respectively; in coupling analysis, they represent the minimum and maximum annual total loads among all parameter combinations, respectively.

2.4. Supplementary Sensitivity and Uncertainty Analysis

To further examine the robustness of the parametric simulation results, Chengdu was selected as a representative city for supplementary parameter sensitivity analysis. Unlike severe cold and cold regions, where low-temperature periods play a more prominent role, and the hot summer–warm winter region, where high-temperature periods are more dominant, the hot summer–cold winter region is characterized by both hot summers and cold winters throughout the year. Therefore, Chengdu can be regarded as a representative case with combined heating and cooling characteristics, and was used to test the stability of the simulation results under perturbations of key parameters.

The supplementary sensitivity analysis was conducted based on the baseline case of Chengdu, with the following reference parameters: external wall insulation thickness of 50 mm, external surface solar absorptivity of 0.5, and air change rate of 0.5 h^{-1}. On this basis, supplementary simulations were carried out from two aspects (Table 5):

1. With the insulation thickness fixed at 50 mm, three intermediate solar absorptivity values of 0.2, 0.4, 0.6 and 0.8 were added to examine the influence of the absorptivity interval on the judgement of load-response trends.
2. Under the conditions of 50 mm insulation thickness, solar absorptivity of 0.5, and the original insulation material, the air change rate was set to 0.4 and 0.6 h^{-1} to examine the stability of model outputs under perturbations in the ventilation boundary condition.

Table 5. Supplementary sensitivity scheme settings.

Type	Parameter Setting	Purpose
Baseline	T = 50 mm, A = 0.5, ACH = 0.5 h^{-1}	Reference
Solar absorptivity	Solar absorptivity A = 0.2	Refined absorptivity interval
	Solar absorptivity A = 0.4	
	Solar absorptivity A = 0.6	
	Solar absorptivity A = 0.8	
Air change rate	Air change rate −20%	Lower-bound ventilation condition
	Air change rate +20%	Upper-bound ventilation condition

Note: T denotes insulation thickness; A denotes exterior surface solar absorptivity; ACH denotes air change rate.

2.5. Carbon Translation of Thermal Loads

To further examine whether the load-optimal envelope configuration also corresponds to the operational-carbon-optimal configuration, this study estimated operational carbon emissions based on the simulated heating and cooling loads. The calculation boundary was limited to carbon emissions caused by space heating and space cooling during the building operation stage. Embodied carbon emissions associated with envelope material production, transportation, construction, maintenance, replacement, and demolition were not included, nor was life-cycle cost analysis considered.

According to the climate zones and common energy-supply modes of the five representative cities, different conversion methods were adopted for heating and cooling loads. The heating loads of Yinchuan and Beijing were converted using a district-heating emission factor, while the heating loads of Chengdu, Guangzhou, and Kunming were converted based on an electric heat-pump system. The cooling loads of all five cities were converted based on an electric cooling system. To ensure consistency in the calculation basis and comparability among different cities and parameter combinations, all electricity emission factors were taken from the provincial average electricity CO_2 emission factors released in the same year. The calculation methods are as follows.

- Cooling-related carbon emissions were calculated using Equation (7):

$$C_{cool} = \frac{Q_{cool}}{COP_c} \times EF_{grid} \tag{7}$$

- Heating-related carbon emissions for Yinchuan and Beijing were calculated using Equation (8):

$$C_{heat} = Q_{heat} \times EF_{DH} \tag{8}$$

- Heating-related carbon emissions for Chengdu, Guangzhou, and Kunming were calculated using Equation (9):

$$C_{heat} = \frac{Q_{heat}}{COP_h} \times EF_{grid} \quad (9)$$

- Total operational carbon emissions were calculated using Equation (10):

$$C_{total} = C_{heat} + C_{cool} \quad (10)$$

where C_{cool}, C_{heat} and C_{total} denote annual cooling-related, heating-related, and total operational carbon emissions ($kgCO_2$), respectively; Q_{cool} and Q_{heat} denote annual cooling and heating loads (kWh), respectively; COP_c and COP_h are the coefficients of performance for cooling and heat-pump heating systems, respectively; and EF_{grid} and EF_{DH} represent the electricity and district-heating emission factors, respectively. The main parameters used in the calculation are listed in Table 6.

Table 6. Parameters used for operational carbon emission estimation.

Parameter	Symbol	Value	Source
Cooling system performance coefficient	COP_c	3.0	GB 19577–2024 [33]
Heat-pump heating performance coefficient	COP_h	2.5	
Provincial electricity CO_2 emission factor	EF_{grid}	Ningxia = 0.6187 ($kgCO_2$/kWh)	MEE & NBS, 2023 provincial power CO_2 factors [34]
		Beijing = 0.5554 ($kgCO_2$/kWh)	
		Sichuan = 0.1564 ($kgCO_2$/kWh)	
		Guangzhou = 0.4419 ($kgCO_2$/kWh)	
		Yunnan = 0.1333 ($kgCO_2$/kWh)	
District heating CO_2 emission factor	EF_{DH}	0.396 ($kgCO_2$/kWh)	NDRC GHG accounting guideline [35]
Reference operating condition	-	50–0.5 (T&A)	Defined in this study

Note: Yinchuan, Beijing, Chengdu, Guangzhou, and Kunming correspond to the provincial average electricity CO_2 emission factors of Ningxia, Beijing, Sichuan, Guangdong, and Yunnan, respectively. The district-heating emission factor was converted from 0.11 tCO_2/GJ, equivalent to 0.396 $kgCO_2$/kWh.

3. Result

3.1. Load Characteristics in Different Climate Zones

Figure 4 and Table 7 present the annual heating load, annual cooling load, and their proportional characteristics of residential buildings in the five representative cities. Overall, the annual thermal loads of buildings exhibit pronounced regional differentiation across different climate zones. The heating loads of Yinchuan and Beijing reached 175,477.69 kWh and 150,078.39 kWh, accounting for 74.83% and 65.69% of their respective annual total loads, which indicates a clear heating-dominated pattern. In contrast, Guangzhou recorded a cooling load as high as 161,383.32 kWh, accounting for 98.4% of its annual total load, suggesting that building operation in the hot summer–warm winter region is almost entirely governed by summer cooling demand. In Chengdu and Kunming, the shares of heating and cooling loads were relatively close, with Chengdu showing 53.78% and 46.22%, and Kunming 46.62% and 53.38%, respectively. This indicates that these two regions are jointly influenced by both winter insulation demand and summer heat-shielding demand.

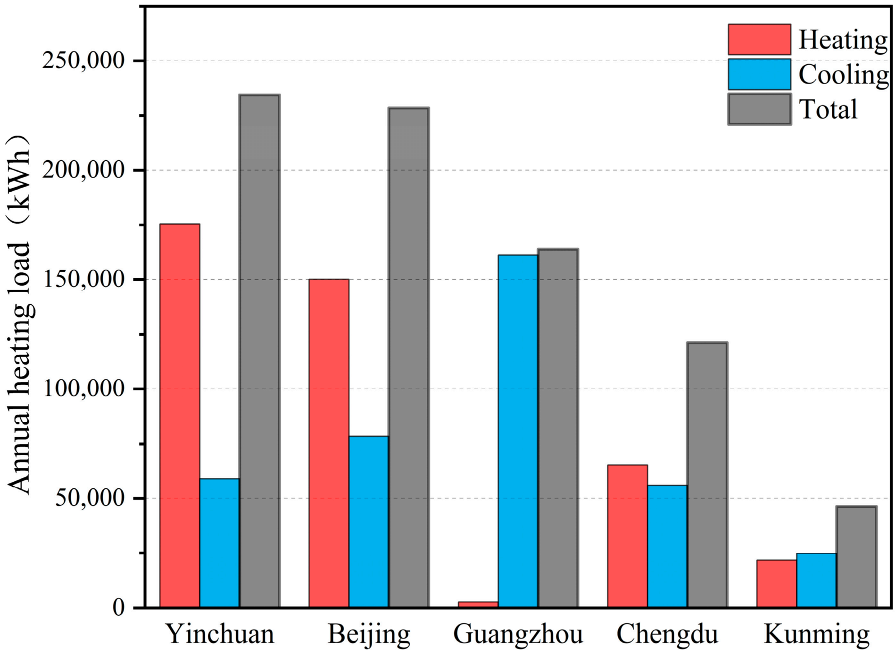

Figure 4. Comparison of heating, cooling, and total loads in five cities.

Table 7. Comparison of load characteristics in five cities.

City	Annual Load (kWh)		Proportion (%)	
	Heating	**Cooling**	**Heating**	**Cooling**
Yinchuan	175,477.69	59,029.31	74.83	25.17
Beijing	150,078.39	78,399.29	65.69	34.31
Chengdu	65,220.53	56,030.19	53.78	46.22
Guangzhou	2627.72	161,383.32	1.60	98.4
Kunming	21,609.12	24,743.87	46.62	53.38

In terms of total magnitude, Yinchuan and Beijing exhibited the highest annual total loads, reaching 234,507.00 kWh and 228,477.68 kWh, respectively, followed by Guangzhou and Chengdu, while Kunming had the lowest value at only 46,352.99 kWh. Overall, as the climate shifts from severe cold and cold regions toward mild regions, the annual total load of residential buildings generally tends to decrease. Further examination of the heating–cooling load composition indicates that when one type of load dominates annual operation, the total building load is often relatively high. Yinchuan and Beijing were dominated by heating load and therefore exhibited high annual total loads; Guangzhou, although overwhelmingly dominated by cooling load, also showed a relatively large total load. By contrast, Chengdu and Kunming had more balanced heating and cooling loads, and their annual total loads were generally lower, with Kunming showing the lowest load level in particular.

3.2. Single-Factor Analysis of Typical Parameters

3.2.1. Effect of External Wall Insulation Thickness

Figure 5 and Table 8 illustrate the variation in building thermal loads in the five cities as the external wall insulation thickness increases from 30 mm to 70 mm. The results show that, with increasing insulation thickness, the heating loads in all five cities decrease significantly, whereas the cooling loads increase to varying degrees. This indicates that enhanced insulation performance helps reduce heat-transfer losses through the envelope in winter, but at the same time weakens the building's ability to dissipate heat outward in summer, thereby increasing cooling demand.

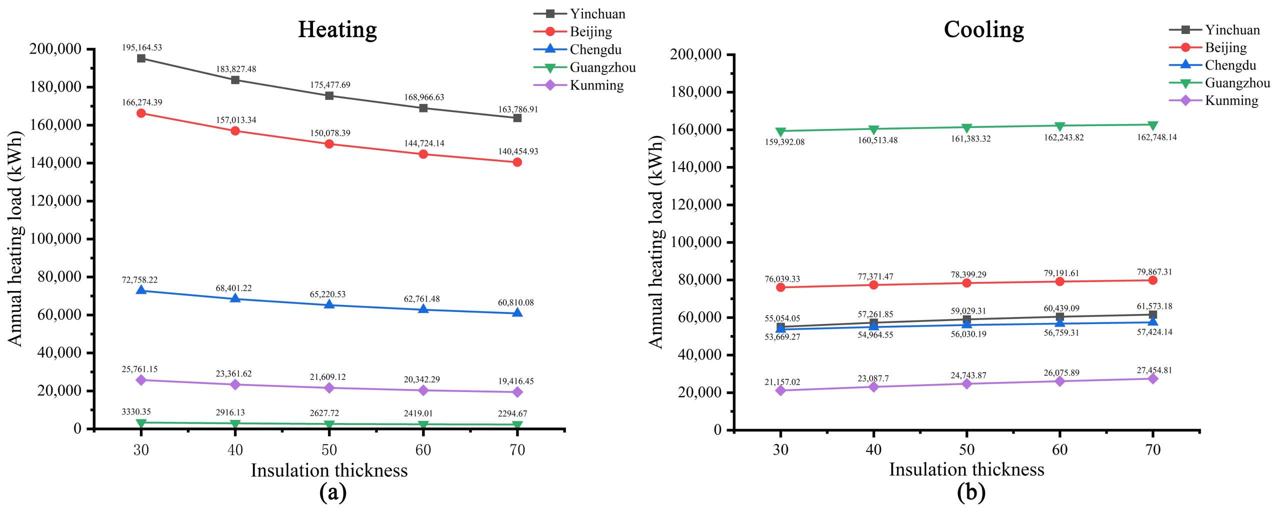

Figure 5. Analysis of loads at different insulation thicknesses. (**a**) Heating. (**b**) Cooling.

Table 8. Load response to insulation thikness.

City	R (%)			S		
	Heating	**Cooling**	**Total**	**Heating**	**Cooling**	**Total**
Yinchuan	−16.08	11.84	−9.93	−0.120	0.089	−0.074
Beijing	−15.53	5.03	−9.08	−0.116	0.038	−0.068
Chengdu	−16.42	7.00	−6.48	−0.123	0.053	−0.049
Guangzhou	−31.10	2.10	1.43	−0.233	0.016	0.011
Kunming	−24.63	29.77	−0.10	−0.185	0.223	−0.001

Although the heating and cooling loads in all cities change in the same direction, the response of annual total load shows clear differences across climate zones. The annual total load decreases by 9.93%, 9.08%, and 6.48% in Yinchuan, Beijing, and Chengdu, respectively, indicating that in the severe cold, cold, and hot summer–cold winter regions, the winter energy-saving benefits brought by increased insulation thickness outweigh the adverse effect of higher cooling loads in summer. This effect is particularly pronounced in Yinchuan and Beijing, where heating dominates annual operation and insulation thickness has the most significant impact on reducing annual total load. In contrast, the annual total load in Guangzhou increases by 1.43% as insulation thickness rises, suggesting that in the hot summer–warm winter region, simply increasing insulation thickness may have a negative effect on year-round energy savings. In Kunming, the annual total load decreases by only 0.10%, indicating that the annual load of buildings in the mild region responds only weakly to changes in insulation thickness.

The normalized sensitivity coefficients further confirm the above pattern. The sensitivity coefficients of annual total load are −0.074, −0.068, and −0.049 for Yinchuan, Beijing, and Chengdu, respectively, all of which are negative, indicating that increasing insulation thickness is generally beneficial for reducing annual total load. In Guangzhou, the sensitivity coefficient of annual total load is 0.011, suggesting that the total load in this region increases with increasing insulation thickness. In Kunming, the sensitivity coefficient is close to zero, at only −0.001, indicating that it is almost insensitive to changes in insulation thickness.

3.2.2. Effect of External Surface Solar Absorptivity

Figure 6 and Table 9 show the variation in building thermal loads in the five cities as the external surface solar absorptivity increases from 0.1 to 0.7. The results indicate that, with increasing solar absorptivity, the heating loads in all five cities decrease slightly, whereas the cooling loads increase.

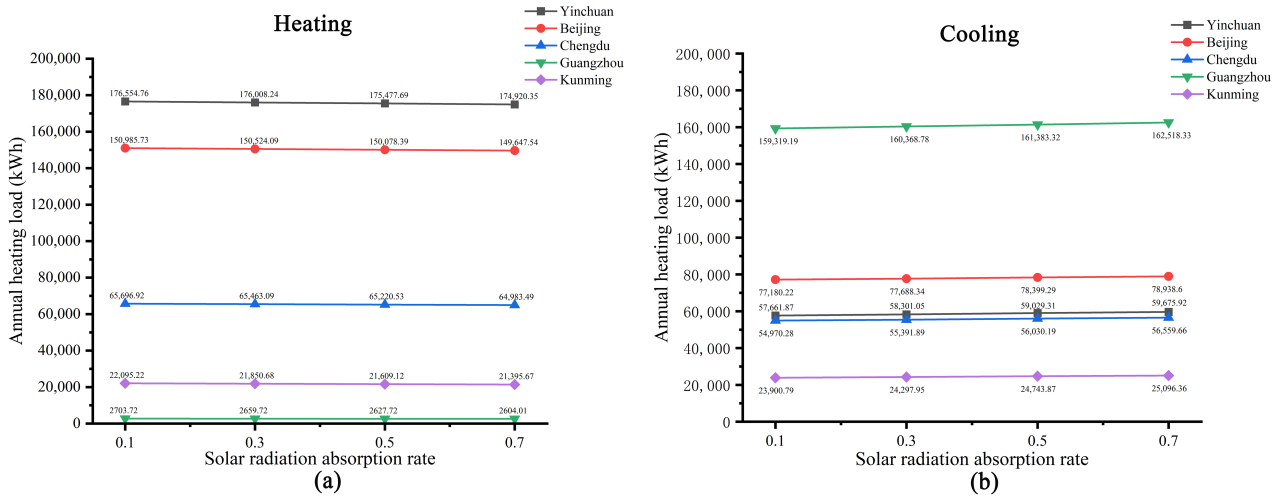

Figure 6. Analysis of loads at different solar absorption rates. (**a**) Heating. (**b**) Cooling.

Table 9. Load response to solar absorptivity.

City	R (%)			S		
	Heating	**Cooling**	**Total**	**Heating**	**Cooling**	**Total**
Yinchuan	−0.93	3.49	0.17	−0.0015	0.0058	0.0003
Beijing	−0.89	2.28	0.19	−0.0015	0.0038	0.0003
Chengdu	−1.09	2.89	0.73	−0.0018	0.0048	0.0012
Guangzhou	−3.69	2.01	1.91	−0.0061	0.0034	0.0032
Kunming	−3.17	5.00	1.08	−0.0053	0.0083	0.0018

In terms of the variation magnitude of annual total load, the response of all cities to changes in solar absorptivity is generally weaker than that to insulation thickness. The annual total loads of Yinchuan and Beijing increase by only 0.17% and 0.19%, respectively, indicating that the annual loads in cold regions are relatively insensitive to the solar-radiation characteristics of the external surface. Chengdu shows an increase of 0.73%, representing a moderate level of response. Guangzhou records the largest increase, at 1.91%, among the five cities, suggesting that in the hot summer–warm winter region, external surface solar absorptivity has a more pronounced influence on annual energy performance. Kunming shows an increase of 1.08%, also reflecting a certain degree of responsiveness.

The sensitivity coefficients further highlight the differences among climate zones. Guangzhou has the largest sensitivity coefficient for annual total load, at 0.0032, indicating the strongest response to changes in solar absorptivity among the five cities. The corresponding values are 0.0018 for Kunming, 0.0012 for Chengdu, and 0.0003 for both Yinchuan and Beijing, suggesting that the influence of external surface solar-radiation characteristics gradually becomes stronger as the climate shifts from heating-dominated to cooling-dominated conditions.

3.3. Coupling Analysis of Typical Parameters

3.3.1. Analysis of Two-Parameter Coupling Effect

Figure 7 presents the distribution of total loads under different thickness–absorptivity combinations in the five cities, while Table 10 lists the maximum total load, minimum total load, total reduction rate, and the corresponding optimal and worst combinations.

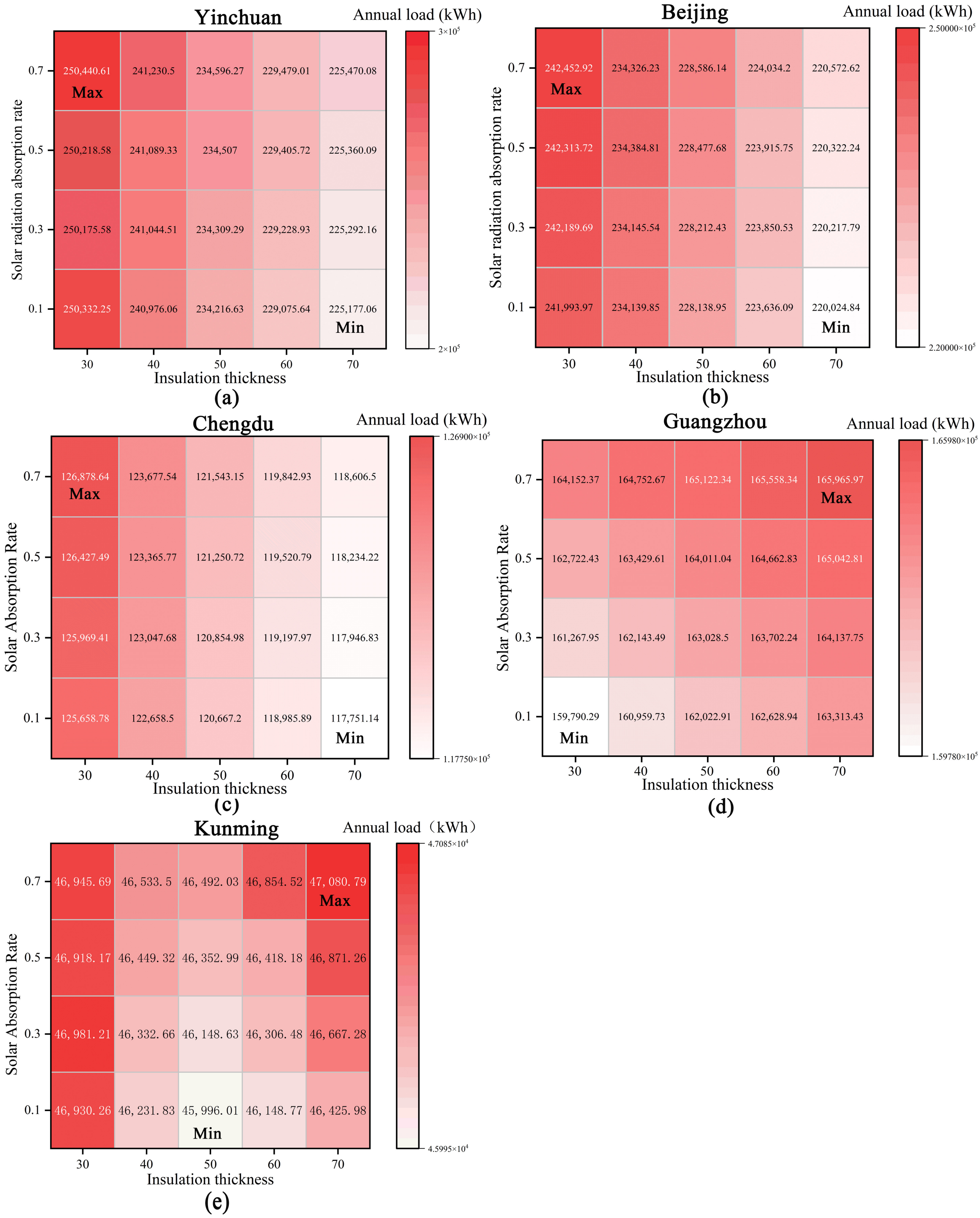

Figure 7. Total load analysis for different parameters combinations in five cities. (**a**) Yinchuan; (**b**) Beijing; (**c**) Chengdu; (**d**) Guangzhou; (**e**) Kunming.

Table 10. Total load analysis for different parameter combinations.

City	Total Load (kWh)		R (%)	Combination (T&A)	
	Max	Min		Best	Worst
Yinchuan	250,440.61	225,177.06	10.09	70-0.1	30-0.7
Beijing	242,452.92	220,024.84	9.25	70-0.1	30-0.7
Chengdu	126,878.64	117,751.14	7.19	70-0.1	30-0.7
Guangzhou	165,965.97	159,790.29	3.72	30-0.1	70-0.7
Kunming	47,080.79	45,996.01	2.30	50-0.1	70-0.7

The results show that the optimal parameter combinations differ significantly across climate zones. In Yinchuan, Beijing, and Chengdu, the minimum total load occurs under the "70 mm + 0.1" combination, whereas the maximum total load occurs under the "30 mm + 0.7" combination, with corresponding total reductions of 10.09%, 9.25%, and 7.19%, respectively. In Guangzhou, the optimal combination is "30 mm + 0.1" and the worst combination is "70 mm + 0.7", with a total reduction of 3.72%. In Kunming, the optimal combination is "50 mm + 0.1" and the worst combination is "70 mm + 0.7", with a total reduction of only 2.30%.

In terms of the combination patterns, the low-value regions in cold and hot summer–cold winter zones are mainly distributed in the range of "high insulation thickness + low solar absorptivity", whereas those in the hot summer–warm winter zone are concentrated in the range of "low insulation thickness + low solar absorptivity". In the mild zone, the optimal range is characterized by a combination of medium insulation thickness and low solar absorptivity.

3.3.2. Analysis of Two-Parameter Coupling Law

To more intuitively illustrate the distribution of annual total load in the parameter space under the combined effects of insulation thickness and external surface solar absorptivity, Figure 8 presents the three-dimensional response surfaces for the representative cities. Among them, Beijing is not shown separately because its variation trend is largely consistent with that of Yinchuan. Compared with two-dimensional heat maps, three-dimensional response surfaces are more helpful for identifying the locations of low-value regions, the dominant gradient directions, and potential nonlinear characteristics.

As can be seen from the response-surface patterns, the low-value regions of Yinchuan and Chengdu are both located near higher insulation thickness and lower solar absorptivity, and the surface gradient is more pronounced along the insulation-thickness direction, indicating that insulation thickness remains the dominant factor governing the distribution of total load in these cities. By contrast, the response surface of Guangzhou rises overall toward the region of higher thickness and higher absorptivity, while its low-value region is concentrated in the range of lower insulation thickness and lower solar absorptivity, suggesting that envelope energy optimization in the hot summer–warm winter region relies more heavily on reducing the solar heat absorption capacity of the external surface. The response surface of Kunming exhibits a relatively distinct local low-value region, with the minimum not occurring at the parameter boundary but near a medium insulation thickness, indicating that the overall response of total load to envelope-parameter variation is relatively weak in mild regions, while still showing certain nonlinear characteristics.

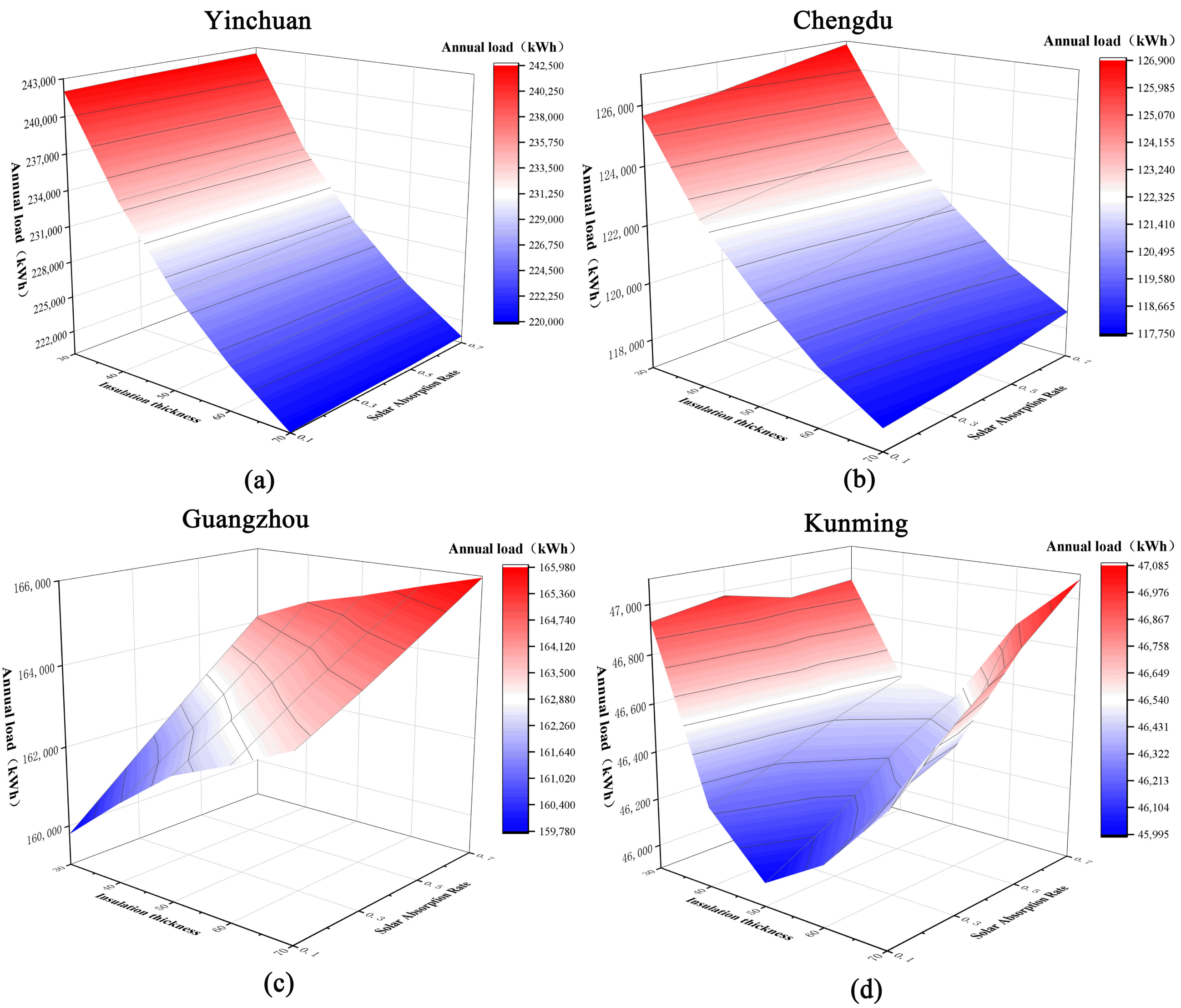

Figure 8. Three-dimensional response surfaces of annual total load in representative cities. (**a**) Yinchuan; (**b**) Chengdu; (**c**) Guangzhou; (**d**) Kunming.

3.4. Results of Supplementary Sensitivity Analysis

As shown in Figure 9, the supplementary sensitivity analysis of external surface solar absorptivity indicates that, as solar absorptivity increases, the heating load decreases while the cooling load gradually increases, and the overall response remains continuous and monotonic. This suggests that the previously identified influence direction of solar absorptivity remains unchanged after introducing intermediate absorptivity levels.

Within the tested range of air change rate, the heating load increases with enhanced ventilation, whereas the cooling load decreases, and the total load rises slightly. This indicates that, in Chengdu, the increase in winter heat loss caused by stronger ventilation outweighs the cooling-load reduction resulting from enhanced summer heat dissipation, leading to a slight increase in annual total load.

Overall, neither type of parameter perturbation causes abrupt changes or trend reversals in load response. All load indicators exhibit stable monotonic variation, indicating good response continuity and robustness of the model under changes in external surface radiation conditions and ventilation boundary conditions.

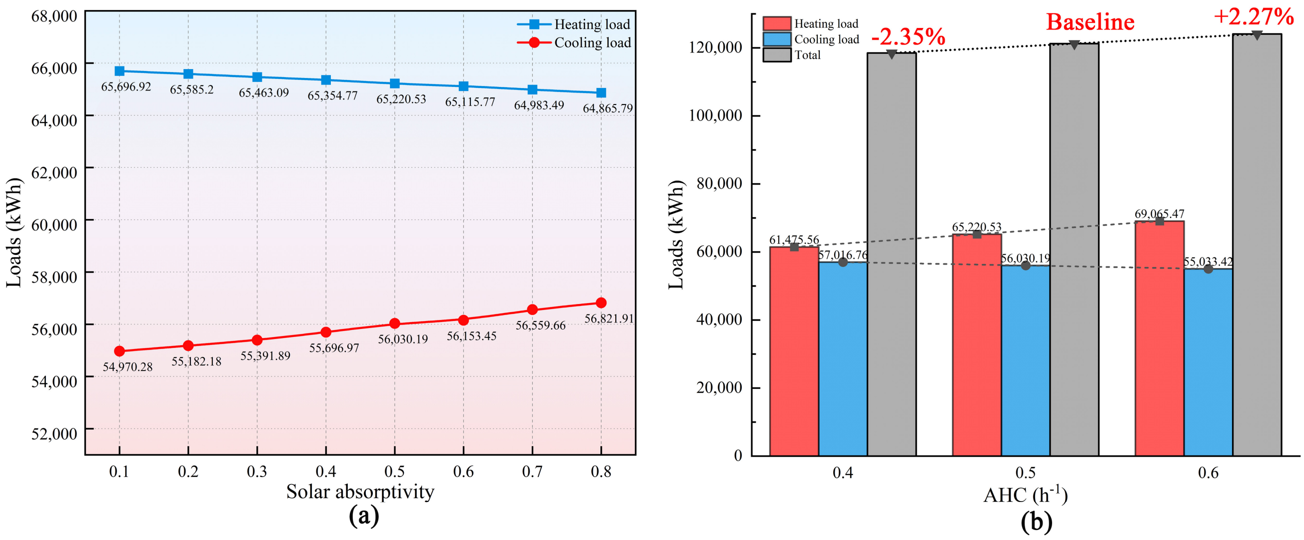

Figure 9. Supplementary sensitivity analysis of key parameters in Chengdu. (**a**) External surface solar absorptivity. (**b**) Air change rate.

3.5. Load-Optimal Versus Carbon-Optimal Configurations

Based on Equations (7)–(10), the annual operational carbon emissions of all parameter combinations in each city were further calculated and re-ranked according to total operational carbon emissions. Table 11 compares the load-optimal and operational carbon-optimal configurations of the five representative cities and presents the carbon reduction rate of the carbon-optimal configuration relative to the baseline case.

Table 11. Comparison between load-optimal and carbon-optimal envelope configurations.

City	Load-Optimal (T&A)	Carbon-Optimal (T&A)	Carbon Reduction (%)	Coincide?
Yinchuan	70-0.1	70-0.7	5.1	No
Beijing	70-0.1	70-0.7	4.82	No
Chengdu	70-0.1	70-0.1	3.31	Yes
Guangzhou	30-0.1	30-0.1	2.46	Yes
Kunming	50-0.1	60-0.1	0.75	No

As shown in Table 11, the load-optimal and carbon-optimal configurations do not fully coincide across the five cities. In Yinchuan and Beijing, the load-optimal configuration is 70-0.1, whereas the carbon-optimal configuration shifts to 70-0.7, indicating that operational carbon evaluation may change the ranking of envelope configurations in heating-dominated regions. In Chengdu and Guangzhou, the two optimal configurations remain consistent, corresponding to 70-0.1 and 30-0.1, respectively. In Kunming, the load-optimal configuration is 50-0.1 and the carbon-optimal configuration is 60-0.1, but the carbon reduction rate is only 0.75%, suggesting a weak carbon-response effect. The results indicate that reducing heating and cooling loads generally helps reduce operational carbon emissions, but the load-optimal configuration does not necessarily correspond to the carbon-optimal configuration.

4. Discussion

4.1. Formation Mechanisms and Climate-Dependent Dominance Transition

Different from previous studies that have mainly focused on whether insulation thickness or solar absorptivity affects building loads [36,37], the present study further shows that the effects of envelope parameters on annual total load are not only strongly climate-dependent, but also characterized by a transition in dominant parameters across different climate zones. The sensitivity coefficients and relative change rates further indicate that the two parameters do not affect annual total load at the same magnitude. The maximum absolute sensitivity coefficient of external wall insulation thickness reaches 0.074, with the corresponding change in total load approaching 10%. In contrast, the sensitivity coefficient of external surface solar absorptivity for annual total load mainly ranges from 0.0003 to 0.0032, corresponding to a total-load change of only 0.17–1.91%. This indicates that insulation thickness remains the dominant factor affecting annual total load in most climate zones, but this dominant relationship does not remain unchanged across all regions.

In heating-dominated regions such as Yinchuan and Beijing, winter heat loss through the building envelope constitutes an important component of annual load. Increasing the insulation thickness of external walls can enhance the thermal resistance of the envelope and reduce winter heat-transfer loss. Although this may also weaken outward heat dissipation in summer to some extent and lead to an increase in cooling load, under heating-dominated conditions, this adverse effect is insufficient to offset the winter energy-saving benefit. Although Chengdu is not a typical heating-dominated city, its heating load still accounts for a relatively large proportion of the annual load; therefore, increasing insulation thickness still shows a pronounced optimization effect on annual total load. It should also be noted that the benefit of increasing insulation thickness is not linear. The diminishing marginal benefit observed in cold regions follows directly from the series structure of envelope thermal resistance. The conductive load scales with the wall transmittance U = 1/R_total, where R_total = R_other + d/λ; each added millimetre of insulation increases R_total linearly, so U—and hence the conductive heating load—declines as 1/ (a + bd), and its reduction per unit thickness falls roughly with the square of accumulated resistance. This explains quantitatively why the heating-load reduction from 30 to 40 mm markedly exceeds that from 60 to 70 mm. The following figure, taking Yinchuan as a representative case, further illustrates the diminishing marginal effect of heating load reduction (Figure 10).

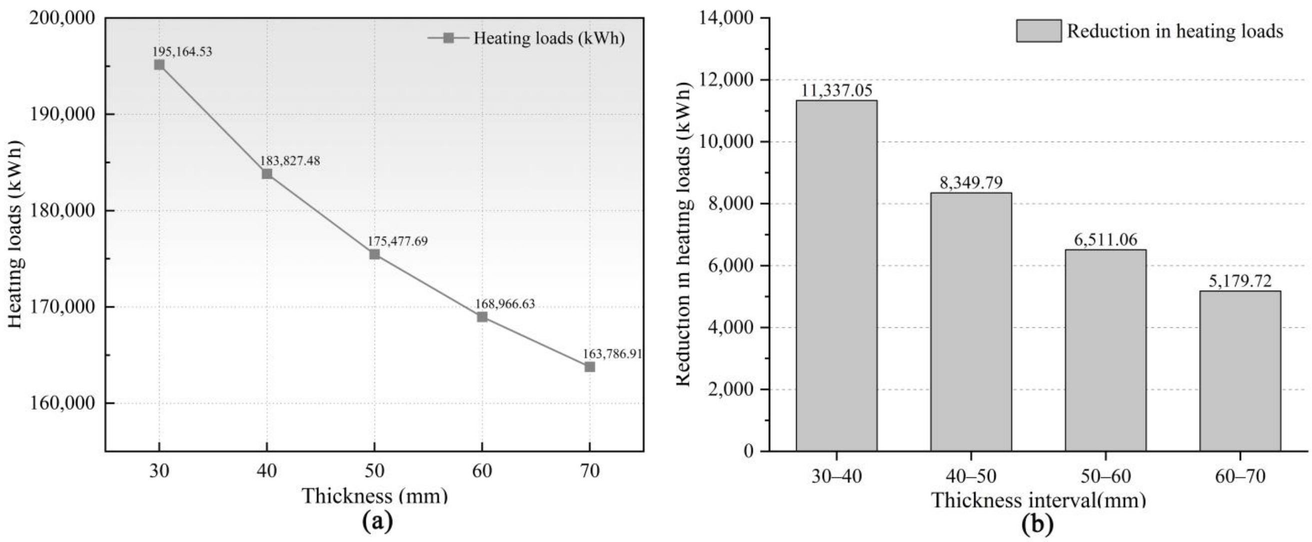

Figure 10. Diminishing marginal effect of heating-load reduction with increasing insulation thickness in Yinchuan: (**a**) heating load under different insulation thicknesses; (**b**) heating-load reduction between adjacent thickness intervals.

In Guangzhou the sign reversal is mechanistically distinct rather than incidental. Because heating constitutes only 1.6% of the annual load, the winter heat-loss-reduction channel through which insulation normally pays off is nearly absent, while the summer channel remains active: added wall resistance impedes the outward dissipation of absorbed and internal heat during the cooling season. With the beneficial channel suppressed and the penalty channel operative, the net annual effect of thickening insulation is adverse—hence the positive total-load sensitivity (S = +0.011). Solar absorptivity, by contrast, acts directly on the dominant summer solar-gain term, which is why it overtakes thickness as the controlling lever in this zone. In Kunming, the near-balance of heating and cooling demand means a parameter change that benefits one load typically penalizes the other, so the two effects largely cancel on an annual basis. This offsetting underlies both the weak overall sensitivity and the interior (non-boundary) optimum at medium thickness evident in the response surface (Figure 8), the only city exhibiting a distinct local minimum.

Overall, low solar absorptivity appears in the optimal configurations of all five cities, indicating that reducing the solar absorption capacity of exterior surfaces represents a relatively consistent optimization direction. This is consistent with previous findings that lower exterior surface absorptivity helps reduce summer solar heat gains [38]. However, this study further shows that the effect magnitude and priority of the two parameters vary across climate zones. Therefore, the key to climate-adaptive envelope design lies not only in identifying optimal configurations, but also in recognizing the transition mechanism of parameter dominance.

4.2. Engineering and Low-Carbon Implications

4.2.1. Low-Carbon Implications of Load–Carbon Divergence

The results in Section 3.5 show that the load-optimal and operational carbon-optimal configurations do not fully coincide in some climate zones. This indicates that reducing building heating and cooling loads generally contributes to lowering operational carbon emissions, but the two cannot be regarded as equivalent. The load-optimal result mainly reflects the building's demand for heating and cooling, whereas operational carbon emissions are also jointly affected by energy supply mode, system efficiency, and regional emission factors. Therefore, the same load variation may correspond to different carbon-reduction benefits across cities and energy systems.

In heating-dominated cities such as Yinchuan and Beijing, the load-optimal configurations are both 70-0.1, whereas the operational carbon-optimal configurations shift to 70-0.7. This suggests that, after introducing operational carbon conversion, the winter solar heat-gain benefit associated with higher solar absorptivity may carry greater weight in the carbon-emission ranking. Although higher absorptivity may increase the cooling load to some extent, in regions with high heating demand and a large share of heating-related carbon emissions, its effect in reducing heating-related carbon emissions may outweigh the adverse increase in summer cooling-related carbon emissions. Therefore, for severe cold and cold regions, low-carbon envelope optimization should not rely solely on minimizing annual total load, but should also incorporate heating energy supply modes and carbon emission factors into the evaluation.

By contrast, the load-optimal and operational carbon-optimal configurations remain consistent in Chengdu and Guangzhou. This indicates good consistency between the directions of reducing heating and cooling loads and reducing operational carbon emissions in these two cities. In Kunming, although the two types of optimal configurations differ slightly, the carbon reduction rate of the carbon-optimal configuration relative to the baseline case is only 0.75%, suggesting that, in mild regions, envelope-parameter variations have a relatively limited influence on operational carbon emissions due to the low overall heating and cooling loads. Therefore, the operational carbon results further highlight the importance of climatic zoning and energy-system differences. Envelope-parameter optimization should not only focus on changes in heating and cooling loads, but also evaluate low-carbon benefits in relation to local energy supply modes and emission factors.

4.2.2. Comparison with Current Building Energy-Efficiency Standards

To further examine the engineering applicability of the simulated optimal results, this study compares the exterior-wall heat transfer coefficient K under the optimal configurations with the current building energy-efficiency standards of the five cities.

As shown in Table 12, the simulated optimal results show both consistency with and divergence from the current building energy-efficiency standards. In Guangzhou, the optimal solution corresponds to a relatively high exterior-wall K value, indicating that in the hot summer–warm winter region, where cooling load is highly dominant, envelope energy-efficiency optimization should not be simply understood as continuously reducing the exterior-wall heat transfer coefficient. Instead, greater attention should be paid to the combined effects of controlling external surface solar absorptivity, improving surface reflectance, and optimizing thermal inertia. The optimal solutions in Chengdu and Kunming both satisfy the corresponding standard limits and show a certain degree of similarity. However, when combined with the preceding load analysis, the optimal K value in Kunming is higher than that in Chengdu, and its load sensitivity is weaker. This suggests that although mild regions can still achieve some energy-saving benefits through a moderate reduction in K value, the marginal effect of further strengthening insulation is relatively limited.

Table 12. Comparison between simulated optimal solutions and reference standards.

City	Reference Standard		Optimal Solution		Findings
	Source	Range	(T&A)	Corresponding K	
Yinchuan	DB64/521-2022 [39]	$K \leq 0.45$	70-0.1	0.409	compliant
Beijing	DB11/891-2020 [40]	$K \leq 0.35$ or 0.23	70-0.1	0.409	Not compliant
Chengdu	Local policies, 2022 [41]	$K \leq 0.60$ when $D \leq 2.5$; $K \leq 0.90$ when $D > 2.5$	70-0.1	0.409	compliant
Guangzhou	JGJ 75-2012 [42]	$K \leq 0.70$ when $D \leq 2.5$; $K \leq 1.50$ when $D > 2.5$;	30-0.1	0.767	Conditional
Kunming	GB 55015-2021 [43]	$K \leq 0.60$ when $D \leq 2.5$; $K \leq 1.00$ when $D > 2.5$	50-0.1	0.578	Compliant

Note: K denotes the exterior-wall heat transfer coefficient, $W/(m^2 \cdot K)$, and D denotes the exterior-wall thermal inertia index.

The K value corresponding to the simulated optimal solution in Yinchuan satisfies the requirements of the Ningxia local standard, indicating that improving exterior-wall insulation in severe cold regions is generally consistent with the control direction of current standards. By contrast, under the same optimal parameter combination, the corresponding K value in Beijing is higher than the limit specified in the Beijing local standard and therefore does not meet this stricter requirement. This difference does not mean that the simulation results contradict engineering practice. Rather, it indicates that local standards reflect not only climate-adaptive requirements, but also regional energy-saving targets, building carbon-emission control requirements, technical routes, and practical implementation conditions. It is worth noting that, if the general limit for residential buildings in cold regions, $K \leq 0.45$ [44], is used as a reference, the K value of the optimal solution in Beijing still falls within this range. This further suggests that the difference between the Beijing simulation result and the local standard may be related to the more stringent requirements of that specific regional standard.

Overall, the simulated optimal K values in multiple cities are generally consistent with the control direction of current energy-efficiency standards, indicating that the envelope-parameter response patterns obtained from the unified model have certain engineering interpretability. At the same time, the differences observed in Beijing and Guangzhou also show that simulated optimal results cannot be directly regarded as code-recommended values. In practical engineering applications, envelope optimization should be based on climate-adaptive analysis and further integrated with local standard limits, thermal inertia requirements, energy supply modes, low-carbon targets, and practical implementation conditions.

4.3. Research Boundaries and Future Work

This study adopts a unified building model, consistent operating boundaries, and a defined envelope-parameter range to conduct cross-climate-zone comparative analysis. The aim is to reveal the relative effects of external wall insulation thickness and external surface solar absorptivity on heating and cooling loads as well as operational carbon emissions under different climatic conditions. By keeping the building prototype, material type, indoor set-point temperatures, air change rate, and carbon-emission conversion parameters consistent, the interference of non-research variables can be reduced, thereby improving the comparability of results among different cities. Therefore, the conclusions of this study are mainly applicable to climate-adaptive comparison and parameter-mechanism analysis within the defined parameter space, rather than directly replacing code-based design requirements or cost-optimal design decisions in specific engineering projects.

In terms of parameter settings, the external wall insulation thickness was set within the range of 30–70 mm, while the insulation material type was kept constant, following the principle of controlled variables. It should be noted that in actual engineering practice, insulation thicknesses in severe cold and cold regions may be further increased according to local standards, material types, and energy-saving targets. Therefore, the optimal thickness identified in this study should be understood as a relative optimum within the unified parameter range, rather than the final recommended thickness for practical applications in each region.

In addition, this study mainly evaluates building heating loads, cooling loads, and their converted operational carbon emissions. The effects of HVAC part-load performance, occupant behavior, construction quality, embodied carbon, life-cycle carbon emissions, and economic performance have not yet been fully incorporated. Future research may extend the present framework by including more city samples, different envelope materials, wider parameter ranges, measured operational data, and multiple HVAC system scenarios, thereby developing a multi-objective optimization model that considers thermal loads, operational carbon emissions, embodied carbon, and economic costs.

5. Conclusions

Based on a unified DeST residential building model, this study compared the effects of external wall insulation thickness and external surface solar absorptivity on building heating and cooling loads as well as operational carbon emissions across five representative climate zones in China. The main conclusions are as follows:

1. A unified cross-climate-zone comparative framework for envelope parameters was established. Different from previous studies that mainly focused on a single parameter or a specific region, this study placed external wall insulation thickness and external surface solar absorptivity within the same building prototype, operating boundaries, and evaluation system. This improved the horizontal comparability of simulation results across different climate zones and provided a unified analytical pathway for identifying how climatic conditions influence the response of envelope parameters.

2. The differences in effect magnitude and the transition of parameter dominance were quantitatively revealed. External wall insulation thickness is the main control parameter affecting annual total load in severe cold, cold, and hot summer–cold winter regions. However, in cooling-dominated regions such as Guangzhou, its effect direction reverses, and external surface solar absorptivity becomes the parameter with higher control priority. This indicates that the key to climate-adaptive design lies not only in identifying optimal combinations, but also in recognizing changes in parameter dominance across different climate zones.
3. Envelope-parameter optimization should not follow a uniform strategy. Low solar absorptivity appears in the optimal configurations of all five representative cities, indicating a relatively consistent cross-climate optimization direction. In contrast, insulation thickness is more climate-zone sensitive and should be configured differently according to local heating and cooling load structures. The results for Guangzhou and Kunming further suggest that envelope optimization should shift toward parameter-priority judgement based on climate-zone-specific load structures.
4. The load optimization results were further translated into operational carbon emissions and standard constraints. The load-optimal configuration does not necessarily correspond to the operational carbon-optimal configuration, and simulated optimal results cannot directly replace local standard limits. Therefore, envelope optimization in practical engineering should comprehensively consider building load response, energy-system efficiency, regional emission factors, and local standard requirements.

Overall, the main contribution of this study is the development and verification of a cross-climate-zone envelope-parameter comparison and engineering translation method. The study clarifies the differences in effect magnitude, the transition of parameter dominance, and the low-carbon applicability boundaries of external wall insulation thickness and external surface solar absorptivity under different climatic conditions, providing a quantitative basis for parameter-priority judgement in residential building energy-efficient design and low-carbon retrofit.

Author Contributions: Y.Y.: Conceptualization, Methodology, Software, Formal analysis, Visualization, Writing—original draft; J.Z.: Investigation, Validation, Data curation, Visualization; Z.J.: Methodology, Validation, Writing—review and editing; Y.L.: Supervision, Resources, Project administration, Writing—review and editing; Q.Y.: Conceptualization, Funding acquisition, Supervision, Project administration, Writing—review and editing. All authors have read and agreed to the published version of the manuscript.

Funding: This research was funded by the Fundamental Research Funds for the Central Universities of China, Southwest Minzu University (Grant No.: ZYN2025069, ZYN2026253), the Sichuan Science and Technology Program (Grant Number: 2025ZNSFSC1309), the Research Center for the Community of the Chinese Nation, National Ethnic Affairs Commission, Southwest Minzu University (Grant No.: 2025JDYB07), China-Portugal Belt and Road Joint Laboratory on Cultural Heritage Conservation Science (Grant No.: DYY2405).

Data Availability Statement: Data will be available on request.

Conflicts of Interest: The authors declare no conflicts of interest. The funders had no role in the design of the study; in the collection, analyses, or interpretation of data; in the writing of the manuscript; or in the decision to publish the results.

References

1. Rhodes, C.J. The 2015 Paris Climate Change Conference: Cop21. *Sci. Prog.* **2016**, *99*, 97–104. [CrossRef]
2. Baş, H. Energy-Efficient House Design in the Mediterranean Climate. *E3S Web Conf.* **2024**, *546*, 01003. [CrossRef]

3. Yang, L.; Yan, H.; Lam, J.C. Thermal Comfort and Building Energy Consumption Implications—A Review. *Appl. Energy* **2014**, *115*, 164–173. [CrossRef]
4. Juan, Y.-K.; Gao, P.; Wang, J. A Hybrid Decision Support System for Sustainable Office Building Renovation and Energy Performance Improvement. *Energy Build.* **2010**, *42*, 290–297. [CrossRef]
5. Shahnazari, H.; Mhaskar, P.; House, J.M.; Salsbury, T.I. Heating, Ventilation and Air Conditioning Systems: Fault Detection and Isolation and Safe Parking. *Comput. Chem. Eng.* **2018**, *108*, 139–151. [CrossRef]
6. Intergovernmental Panel on Climate Change (IPCC) (Ed.) Buildings. In *Climate Change 2022—Mitigation of Climate Change*; Cambridge University Press: Cambridge, UK, 2023; pp. 953–1048.
7. Kumar Kirme, S.; Kapse, V.S. A Comprehensive Review of Residential Building Energy Efficiency Measures in India. *Energy Build.* **2024**, *319*, 114537. [CrossRef]
8. Amani, N. Energy Efficiency of Residential Buildings Using Thermal Insulation of External Walls and Roof Based on Simulation Analysis. *Energy Storage Sav.* **2025**, *4*, 48–55. [CrossRef]
9. Alfarawi, S.; Omar, H.; El-Sawi, A.; Jubori, A.A. Thermal Performance Assessment of External Wall Construction for Energy-Efficient Buildings. *Eur. J. Sustain. Dev. Res.* **2022**, *6*, em0189. [CrossRef] [PubMed]
10. Pan, D.; Chan, M.Y.J.; Deng, S.; Lin, Z. The Effects of External Wall Insulation Thickness on Annual Cooling and Heating Energy Uses under Different Climates. *Appl. Energy* **2012**, *97*, 313–318. [CrossRef]
11. Ozel, M. The Influence of Exterior Surface Solar Absorptivity on Thermal Characteristics and Optimum Insulation Thickness. *Renew. Energy* **2012**, *39*, 347–355. [CrossRef]
12. An, J.; Yan, D.; Cui, Y.; Xiao, C. *Climate Change and Its Impact on Building Energy Consumption in Office Building of Different Climate Zones in China*; IBPSA: Verona, WI, USA, 2017; Volume 15, pp. 1614–1621.
13. Wang, M.; Sunaga, N. The Effects of Building Performance and Air-Conditioning Setting Temperature on Energy Consumption and Thermal Comfort in Multi-Residential Buildings in China. *J. Environ. Eng. (Trans. AIJ)* **2017**, *82*, 347–355. [CrossRef]
14. Zhang, L.Y.; Jin, L.W.; Wang, Z.N.; Zhang, J.Y.; Liu, X.; Zhang, L.H. Effects of Wall Configuration on Building Energy Performance Subject to Different Climatic Zones of China. *Appl. Energy* **2017**, *185*, 1565–1573. [CrossRef]
15. Yuan, J.; Farnham, C.; Emura, K. Optimum Insulation Thickness for Building Exterior Walls in 32 Regions of China to Save Energy and Reduce CO_2 Emissions. *Sustainability* **2017**, *9*, 1711. [CrossRef]
16. Kaynakli, O. A Review of the Economical and Optimum Thermal Insulation Thickness for Building Applications. *Renew. Sustain. Energy Rev.* **2012**, *16*, 415–425. [CrossRef]
17. Kontoleon, K.J.; Eumorfopoulou, E.A. The Influence of Wall Orientation and Exterior Surface Solar Absorptivity on Time Lag and Decrement Factor in the Greek Region. *Renew. Energy* **2008**, *33*, 1652–1664. [CrossRef]
18. Košir, M.; Pajek, L.; Iglič, N.; Kunič, R. A Theoretical Study on a Coupled Effect of Building Envelope Solar Properties and Thermal Transmittance on the Thermal Response of an Office Cell. *Sol. Energy* **2018**, *174*, 669–682. [CrossRef]
19. Rosado, P.J.; Levinson, R. Potential Benefits of Cool Walls on Residential and Commercial Buildings across California and the United States: Conserving Energy, Saving Money, and Reducing Emission of Greenhouse Gases and Air Pollutants. *Energy Build.* **2019**, *199*, 588–607. [CrossRef]
20. Yan, D.; Xia, J.; Tang, W.; Song, F.; Zhang, X.; Jiang, Y. DeST—An Integrated Building Simulation Toolkit Part I: Fundamentals. *Build. Simul.* **2008**, *1*, 95–110. [CrossRef]
21. Yan, D.; Zhou, X.; An, J.; Kang, X.; Bu, F.; Chen, Y.; Pan, Y.; Gao, Y.; Zhang, Q.; Zhou, H.; et al. DeST 3.0: A New-Generation Building Performance Simulation Platform. In *Building Simulation*; Tsinghua University Press: Beijing, China, 2022; Volume 15, pp. 1849–1868. [CrossRef]
22. Pan, L.; Xu, Q.; Nie, Y.; Qiu, T. Analysis of Climate Adaptive Energy-Saving Technology Approaches to Residential Building Envelope in Shanghai. *J. Build. Eng.* **2018**, *19*, 266–272. [CrossRef]
23. Zhang, Y.; Dang, M.; Chu, C.; Behrens, P.; Berrill, P.; Zhong, X.; Jing, R.; Lei, N.; Jia, H.; Zhang, L.; et al. The Climate Opportunities and Risks of Improving Building Envelopes across 1,677 Chinese Cities. *Cell Rep. Sustain.* **2024**, *1*, 100269. [CrossRef]
24. Duan, M.; Sun, H.; Wu, Y.; Wu, X.; Lin, B. Climate Adaptive Thermal Characteristics of Envelope of Residential Passive House in China. *J. Cent. South Univ.* **2022**, *29*, 2317–2329. [CrossRef]
25. Meng, X.; Wei, B.; Zhai, Y. Sensitivity Analysis of Envelope Design Parameters of Industrial Buildings with Natural Ventilation. *Sustainability* **2020**, *12*, 10288. [CrossRef]
26. Peng, C.; Wang, L.; Zhang, X. DeST-Based Dynamic Simulation and Energy Efficiency Retrofit Analysis of Commercial Buildings in the Hot Summer/Cold Winter Zone of China: A Case in Nanjing. *Energy Build.* **2014**, *78*, 123–131. [CrossRef]
27. *GB 50176-2016*; Code for Thermal Design of Civil Buildings. China Architecture & Building Press: Beijing, China, 2016.
28. Li, M.; Xiong, M.; Xiang, C.; Cao, J. How Climate Change Impacts Energy Load Demand for Commercial and Residential Buildings in a Large City in Northern China. *Pol. J. Environ. Stud.* **2018**, *27*, 2133–2141. [CrossRef] [PubMed]
29. Mourshed, M. Relationship between Annual Mean Temperature and Degree-Days. *Energy Build.* **2012**, *54*, 418–425. [CrossRef]

30. Zhao, G.; Zhou, X.; Li, Y.; Sun, C. Dataset of Cooling and Heating Degree Days in North of 18 °N Latitude of China (1981–2020). *J. Glob. Change Data Discov.* **2022**, *3*, 459–466. [CrossRef]
31. National Meteorological Information Center; China Meteorological Administration. China Meteorological Data Service Center: Daily Near-Surface Meteorological Dataset, 2015–2024. Available online: https://data.cma.cn/data/detail/dataCode/A.0012.0001.html (accessed on 29 June 2026).
32. Xu, C.; Shao, S.; Wei, W.; Qin, Y.; Li, N. A Study on Optimum Insulation Thickness of Building Walls in Hot Summer and Warm Winter Zone in China. *Sci. Rep.* **2025**, *15*, 10307. [CrossRef] [PubMed]
33. *GB 19577-2024*; Minimum Allowable Values of the Energy Efficiency and Energy Efficiency Grades for Heat Pumps and Water Chillers. Standards Press of China: Beijing, China, 2024.
34. Ministry of Ecology and Environment of the People's Republic of China; National Bureau of Statistics. Announcement on the Release of 2023 Electricity Carbon Dioxide Emission Factors. Available online: https://www.mee.gov.cn/xxgk2018/xxgk/xxgk01/202512/t20251231_1139517.html (accessed on 30 June 2026).
35. General General Office of the National Development and Reform Commission. Notice on Issuing the Third Batch of Greenhouse Gas Accounting Methods and Reporting Guidelines for Ten Industries. Available online: https://www.ndrc.gov.cn/xxgk/zcfb/tz/201511/t20151111_963496.html (accessed on 30 June 2026).
36. Liu, Z.; Hou, J.; Zhang, L.; Dewancker, B.J.; Meng, X.; Hou, C. Research on Energy-Saving Factors Adaptability of Exterior Envelopes of University Teaching-Office Buildings under Different Climates (China) Based on Orthogonal Design and EnergyPlus. *Heliyon* **2022**, *8*, e10056. [CrossRef] [PubMed]
37. Verichev, K.; Zamorano, M.; Fuentes-Sepúlveda, A.; Cárdenas, N.; Carpio, M. Adaptation and Mitigation to Climate Change of Envelope Wall Thermal Insulation of Residential Buildings in a Temperate Oceanic Climate. *Energy Build.* **2021**, *235*, 110719. [CrossRef]
38. Xu, F.; Zhang, J.J.; Gao, Z.; Tian, D.; Wang, H. Study on the Energy-Saving Effects of Radiative Material Properties and Material Coating Ratios in Residential Neighborhoods with Different Morphologies. *Energy Build.* **2023**, *301*, 113718. [CrossRef]
39. *DB64/521-2022[S/OL]*; Design Standard for Energy Efficiency of Residential Buildings. Ningxia Hui Autonomous Region Department of Housing and Urban-Rural Development: Yinchuan, China, 2022.
40. *DB11/891-2020[S/OL]*; Design Standard for Energy Efficiency of Residential Buildings. Beijing Municipal Commission of Planning and Natural Resources: Beijing, China, 2020.
41. Chengdu Municipal Bureau of Housing and Urban-Rural Development. *Guidelines and Review Key Points for Energy Efficiency Design of Civil Buildings in Chengdu: 2022 Edition[S/OL]*; Chengdu Municipal Bureau of Housing and Urban-Rural Development: Chengdu, China, 2022.
42. *JGJ 75-2012[S/OL]*; Design Standard for Energy Efficiency of Residential Buildings in Hot Summer and Warm Winter Zone. China Architecture & Building Press: Beijing, China, 2012.
43. *GB 55015-2021[S/OL]*; General Code for Building Energy Efficiency and Renewable Energy Application. China Architecture & Building Press: Beijing, China, 2021.
44. *JGJ 26-2018[S/OL]*; Design Standard for Energy Efficiency of Residential Buildings in Severe Cold and Cold Zones. China Architecture & Building Press: Beijing, China, 2018.